doi: 10.5028/jatm.v9i2.623

Performance and Wake Analysis of Rotors in Axial Flight Using Computational Fluid Dynamics

Nik Ahmad Ridhwan Nik Mohd[1], George Barakos[2]

ABSTRACT: Flow field around rotors in axial flight is known to be complex especially in steep descent where the rotor is operating inside its own wake. It is often reported that, in this flight condition, the rotor is susceptible to severe wake interactions causing unsteady blade load, severe vibration, loss of performance, as well as poor control and handling. So far, there is little data from experimental and numerical analysis available for rotors in axial flight. In this paper, the steady Reynolds-Averaged Navier-Stokes Computational Fluid Dynamics solver Helicopter Multi-Block was used to predict the performance of rotors in axial flight. The main objective of this study was to improve the basic knowledge about the subject and to validate the flow solver used. The results obtained are presented in the form of surface pressure, rotor performance parameters, and vortex wake trajectories. The detailed velocity field of the tip vortex for a rotor in hover was also investigated, and a strong self-similarity of the swirl velocity profile was found. The predicted results obtained when compared with available experimental data showed a reasonably agreement for hover and descent rate, suggesting unsteady solution for rotors in vortex-ring state.

KEYWORDS: Axial flight, CFD, Performance, Rotor, Wake structure.

INTRODUCTION

In axial flight, particularly in steep descent where helicopter enters vortex-ring state (VRS), a rotor descends into its own wake. VRS is one of the extreme axial flight conditions and a potentially hazardous flight regime of operation where rotor blades are known to experience severe thrust fluctuations, highly unsteady blade airloads, aperiodic blade flapping, severe vibration, and sudden loss of aircraft altitude and control (Drees and Hendal 1951; Brinson and Ellenrieder 1998; Conlisk 2001; Leishman 2006; Brand *et al*. 2011). This problem is even more dangerous when helicopters operate close to the ground, which may cause unwanted accidents.

Several experiments and computational studies for low speed descending flight have been reported in literature, but relatively a few show detailed quantitative measurements of rotor performance and blade aerodynamic characteristics. Drees and Hendal (1951) are among the first to capture the flow field around rotors in axial flight. The airflow near a rotor installed in the wind tunnel was made visible by using a number of smoke generators. From the experiment, a large flow circulation was captured at the tip of the blade in VRS, and a periodic tumbling motion of the rotor was observed. Another study on measuring rotor performance in axial flight was carried out by Caradonna (1999). The climb performance of a scale model of UH-1H rotor was measured in the wind tunnel at a constant blade tip speed combined with various climb rates and blade collective pitch angles. The rotor cyclic was not considered throughout the test, and the results were

1.Universiti Teknologi Malaysia – Faculty of Mechanical Engineering – Aeronautical Laboratory – Johor Bahru/Johor – Malaysia. **2.**University of Glasgow – School of Engineering – CFD Laboratory – Glasgow – Scotland.

Author for correspondence: Nik Ahmad Ridhwan Nik Mohd | Universiti Teknologi Malaysia – Faculty of Mechanical Engineering – Aeronautical Laboratory | 81310 Skudai | Johor Bahru/Johor – Malaysia | Email: ridhwan@utm.my

Received: Apr. 22, 2016 | **Accepted:** Sept. 16, 2016

also compared to the HELIX-I code. The experimental results provided good quantitative rotor performance and a wake geometry database for Computational Fluid Dynamics (CFD) validation. The difficulties to get accurate rotor performance in hover from experiments, however, required an extrapolation technique to the limit of 0 climb speed. Instead of using a wind tunnel, Washizu *et al.* (1966) used a towing basin to measure a single rotor performance in axial flight. The use of large towing basin in their research was intended to eliminate blockage effects encountered in wind tunnels with closed test sections. Rotor performance for a range of descent speeds was presented in the form of a polar curve and compared with momentum theory. There are several other experiments on scaled rotor in axial flight (Green *et al.* 2005; McAlister *et al.* 2001). Brinson and Ellenrieder (1998) concluded that the entry to the fully developed vortex ring state was found to be sensitive to tunnel velocity and large changes in cyclic required to trim. Due to the extremely complex flow field near the rotor and the lack of data, rotor blade aerodynamics in axial flight is still not well understood.

A number of computer researches to model helicopter flow fields have also been reported. However, most of these focused on hover and forward flight, and only a few on axial flight. The PHIDIAS project provided a platform for the numerical simulation of the 6075 Dauphin VRS and windmill-brake states (WBS) (Bailly 2010). The HOST method was compared with the time-marching, unsteady wake model developed by MINT and flight test data conducted by ONERA at the CEV French Flight Centre. Most of computational fluid dynamics (CFD) solvers developed for rotor aerodynamic simulation are based on solving the Reynolds-Averaged Navier-Stokes equation and are susceptible to excessive numerical dissipation of vorticity on coarse meshes. If not controlled, this dissipation leads to the loss of coherence of vortical structures within the flow. To control this numerical dissipation and dispersion of vorticity in the flow field, a vorticity transport model was developed and tested on rotor in descent (Ahlin and Brown 2005; Line and Brown 2004).

In this study, the Helicopter Multi-block (HMB) CFD solver has been used to compute the performance of rotors at various rates of descent. The main objectives of this paper are to improve basic knowledge of rotor aerodynamics and to validate the flow solver. The results obtained are presented as surface pressure, rotor performance parameters, and vortex wake trajectories. The detailed velocity field of the tip vortex for rotor in hover is also investigated, and a strong self-similarity of the swirl velocity profile is found. The predicted results obtained were compared with available experimental data and showed a reasonably agreement for hovering and moderate rate of descent.

CFD FLOW SOLVER

The description of the HMB is discussed in detail by Barakos *et al.* (2005) and Steijl *et al.* (2006), being briefly presented in this paper. HMB is a computational fluid dynamic Navier-Stokes solver developed at the CFD Laboratory of the University of Liverpool and runs on parallel distributed memory computers. HMB solves the 3D Unsteady Reynolds-Averaged Navier-Stokes (URANS) equations on multi-block structured meshes using a cell-centred finite-volume method for spatial discretisation. In this study, the convective terms are discretised using the Osher's scheme. The Monotone Upstream-centred Schemes for Conservation Laws (MUSCL) interpolation is used to provide formally 3rd-order accuracy in the calculation of fluxes. The van Albada limiter is used to avoid spurious oscillation in the flow properties across shocks by locally reducing the accuracy of the numerical scheme to first order. The resulting linear system of equations is solved using a pre-conditioned Generalised Conjugate Gradient method in conjunction with a Lower Upper factorisation. For unsteady simulations, implicit dual-time stepping is used based on Jameson's pseudo-time integration approach. The viscous computations use the k-ω baseline (BSL) and the Shear Stress Transport (SST) turbulence model of Menter (1994). The SST blends the k-ω model for the inner boundary layer with the k-ε model for the outer boundary layer. Furthermore, the redefined SST eddy viscosity accounts for the effect of transport of turbulent shear stress. The SST model has been used for many external flows with adverse pressure gradients. The solver also has been used and validated for several fundamental flows apart from rotor cases (Badcock *et al.* 2000; Gagliardi and Barakos 2008).

Hovering rotor flow simulations are performed by assuming that the wake shed from the rotor is steady. The hover formulation of HMB allows the computation of hovering rotor flows to be treated as steady-state cases. The formulation uses a mesh that does not rotate and employs a transformation of the frame of reference to account for the rotation. Applying periodic boundaries, an n-bladed rotor can be approximated using a $1/n$ domain segment. The details of the hover formulation

can be found in Steijl *et al.* (2006). For hovering and climbing rotor cases, the momentum based far field boundary model, assuming a three-dimension source-sink singularity at the rotor axis of rotation and at a rotor plane was used (Steijl *et al.* 2006; Srinivasan 1993). For ascending and descending rotor, the vertical velocity is added to the hover velocity. The Froude/Source-sink condition typically used (Steijl *et al.* 2006) for applying the boundary conditions in hover and descending flight at moderate speeds was not adequate for the extreme cases considered here. Therefore, in this paper, for extreme case in descending flight, a free-stream condition was assumed at the far field. For more efficient computations, the vortex-tube model that valid for most of axial flight condition can be used (Wang 1990; Perry *et al.* 2007; Nik Mohd and Barakos 2010).

CFD MESH GENERATION AND TEST CASES

A structured C-H-H CFD mesh was employed (Fig. 1). An H-type structure was used away from the blades with a C-type structure attached to them. This type of mesh topology allows for accurate viscous computations and can provide a mechanism for pitching the blades, with the near-blade mesh remaining in an undeformed state (Brocklehurst *et al.* 2008). For all meshes, viscous spacing in the direction normal to the blade surface with the first cell located at $10^{-5}c$ above the blade and exponential distribution was employed. For viscous cases, this mesh spacing constructed results in $y^+ < 1$. The rotor centre of rotation is located at the z-axis, the rotor blade is laid on the x-axis, and the quarter chord point is taken at $y = 0$ with the blade leading edge pointing at the positive y-axis. This geometry was used for the construction of the computational meshes for the rotors in axial flight. The rotor hub was modelled as a simple straight cylinder. Summary of rotor geometry and flow condition considered in this study are shown in Table 1.

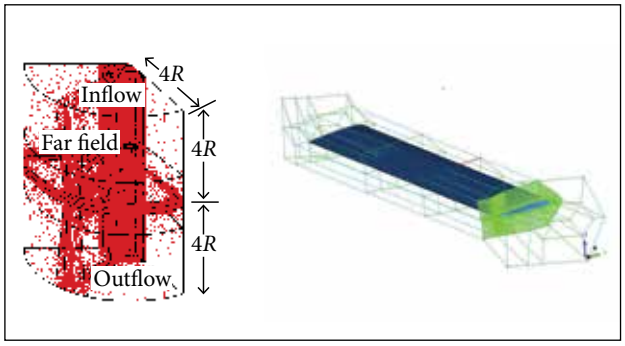

Figure 1. Multi-block mesh employed in HMB.

Table 1. Summary of rotor geometries for axial flight test cases.

Characteristic	UH-1H	Washizu
Rotor geometry		
Number of blades	2	3
Root cut-out	1 c	1 c
Rotor radius	13.67 c	16.67 c (1.1 m)
Chord	1 c	1 c (0.33 m)
Aspect ratio	13.67	16.67
Twist	Untwisted	−8.33°
Solidity	0.047	0.0573
Blade profile	NACA 0012	NACA 0012
Flow condition		
Tip Mach	0.5771	0.1693
Reynolds number ($\times 10^6$)	1.028	0.1306
Grid size ($\times 10^6$)	9	6.3
Number of blocks	170	272
Test case	Hover/climb	Hover/descent

RESULTS AND DISCUSSION

ASCENDING CARADONNA UH-1H ROTOR

For ascending case, the aerodynamic performance and wake geometry of the Caradonna UH-1H rotor were computed for a range of ascend rates, V_v/V_{tip}, from hover to ascending rate of 0.04. The results are presented for a blade at trimmed and untrimmed conditions. For untrimmed condition, the rotor blade collective pitch angle, θ_o, was set at 11° as in Caradonna (1999) experiment. For trimmed conditions, the thrust required for ascend was maintained constant closed to the hover state (Fig. 2a). This is done by considering the incremental of the blade collective pitch settings by 3/4 V_v/Vt_{ip} (Johnson 1980). The coning angle was set at 0 for all calculations. For the ascending test cases considered, the linear increments in the blade collective pitch resulting from the trimmed conditions are plotted in Fig. 2b. The blade tip Mach number was $M_{tip} = 0.5771$ and the Reynolds number, $Re = 1.028 \times 10^6$.

Rotor trimming requires an increment in blade collective pitch angle to maintain the rotor thrust as the ascend speed ratio is increased. This also results in an increment of the rotor torque required (Fig. 2c). For the test cases considered, the rotor losses its efficiency in ascending flight. Comparison with the experimental measurements (Fig. 2d) shows that HMB underpredicts rotor figure of merit (FM) but is in good agreement with HELIX-I data for ascending cases.

Predictions of hover FM were successfully presented in Nik Mohd *et al.* (2011) for the case of Caradonna and Tung (1981). There are, however, some discrepancies for the UH-1H rotor for both HMB and HELIX-I data. In experiments, the drop in the value of FM is expected due to excessive flow unsteadiness (Caradonna 1999), and extrapolation to ascend was suggested to correct the hover FM. The predicted hover FM shows a linear trend; however, the value of the FM falls between the experiments and the HELIX-I data. Overall, for the ascending rotor, the predicted rotor performance without trimming is in excellent agreement with experiments and HELIX-I data. Nevertheless, when the rotor trim condition is activated, a slight increase is observed in the rotor FM for the fast ascending case (Fig. 2d).

Figures 3a to 3d show the blade surface pressure coefficient, C_P, at 3 blade stations plotted for different ascend rates. From the comparison, the blade surface pressure is found to have the same stagnation values, but decreasing suction pressure, as rotor ascend rate increases. The distributions of spanwise blade lift

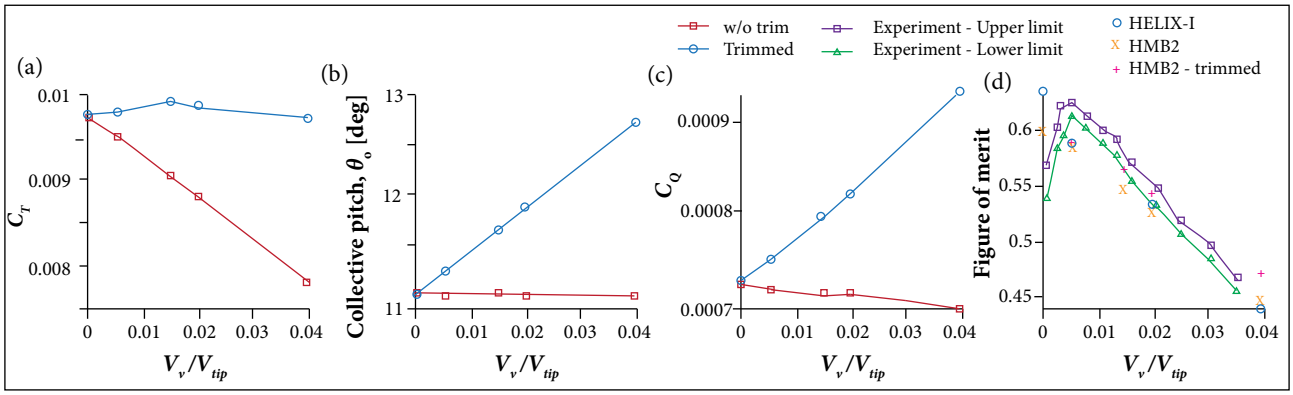

Figure 2. Performance of the Caradonna UH-1H rotor in hover and vertical ascent. (a) Thrust coefficient; (b) Collective pitch; (c) Torque coefficient; (d) Figure of merit.

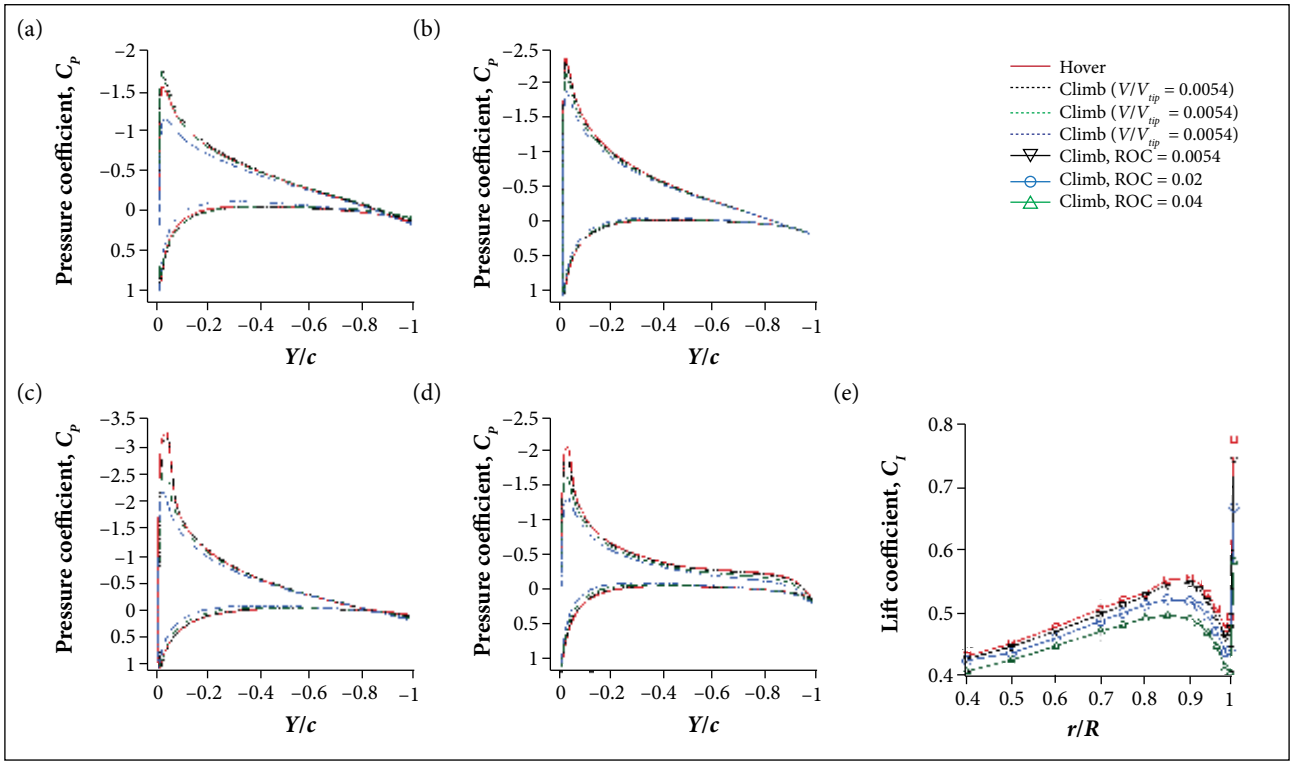

Figure 3. Comparison of CFD results of the Caradonna UH-1H blade surface pressure coefficients at different ascent rates. (a) r/R = 0.30; (b) r/R = 0.70; (c) r/R = 0.90; (d) r/R = 0.99; (e) Lift coefficient. ROC: Rate of climb.

coefficient, C_L, are presented in Fig. 3e and were obtained by integrating the C_P. From the figure, the spanwise C_L is found shifted vertically downwards as the normalised ascending velocity increases from hover to 0.04.

The vertical and axial rotor tip vortex trajectories obtained from CFD, and compared with the No. 1 blade of (Caradonna 1999) experiment are shown in Figs. 4a to 4b. It can be seen that, for low ascending speed, the calculated wake trajectories are in good agreement with the experimental data of Caradonna (1999). It can also be noted that the overall wake geometry is almost identical or independent of trim conditions. The comparison of the blade tip vortices for hovering and ascending flight cases represented by superimposed vorticity-cuts taken at $\Psi_w = 0°$ is depicted in Fig. 5, where, for the hovering case of $V_v/Vt_{ip} = 0$, the primary blade tip vortex of blade No. 1 after a complete revolution is predicted to be at 0.927 chord downstream the rotor plane. For a low ascending flight case of $V_v/Vt_{ip} = 0.04$, the primary blade tip vortex predicted by HMB is found to be displaced 2.634 chord downstream the rotor plane. However, due to the fast growth in the mesh spacing due to the exponential distribution used has resulted in a quick dissipation and dispersion of vorticity field.

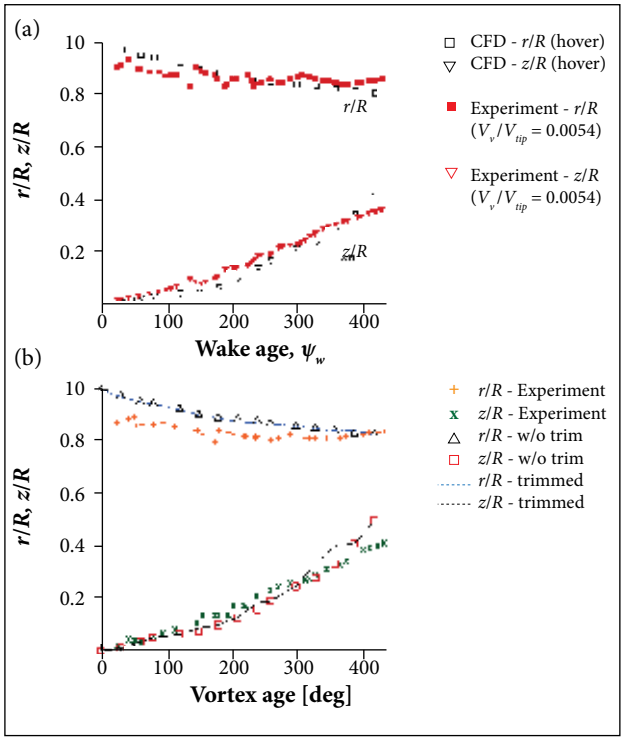

Figure 4. Normalised radial (r/R) and vertical (z/R) displacement of rotor tip vortex for $\theta_{0.7} = 11°$ and $M_{tip} = 0.5771$.(a) Hover; (b) $V_v/V_{tip} = 0.015$.

The distributions of vortex swirl velocity normalised with the rotor tip speed across the tip vortex cores for various wake ages are shown in Fig. 6. This information also shows how strong the axial velocity induced by the tip vortex is. The vortex swirl velocity of the tip vortex weakens as it evolves

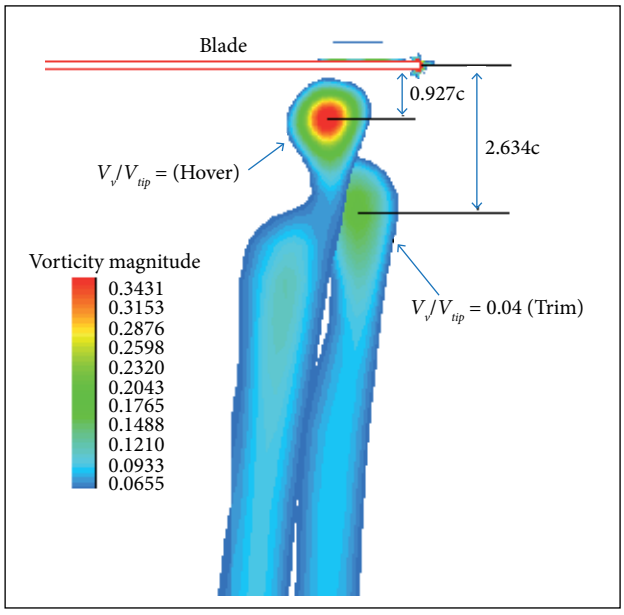

Figure 5. Superimposed vorticity cuts at $\Psi_w = 0°$.

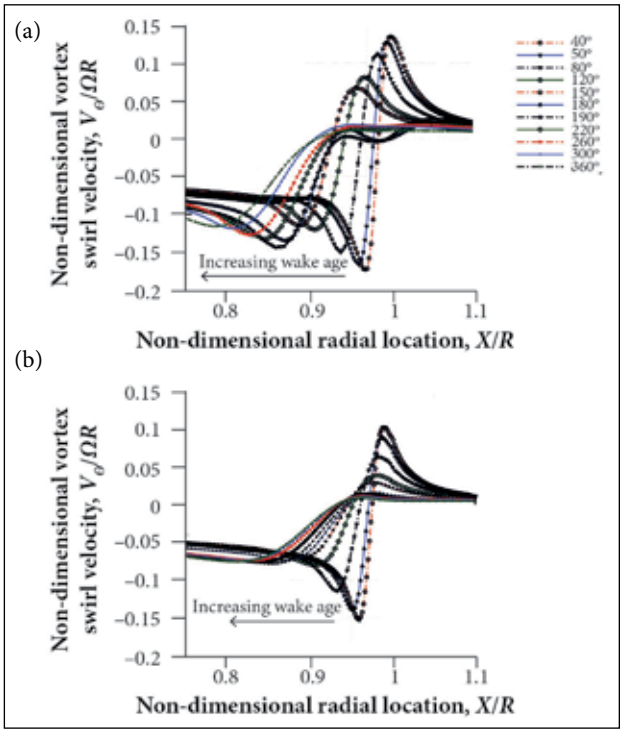

Figure 6. Distribution of vortex swirl velocity of the UH-1H rotor in ascending flight. (a) $V_v/V_{tip} = 0$ (Hover); (b) $V_v/V_{tip} = 0.04$.

but grows in core radius. Furthermore, for the same wake age considered, the vortex swirl velocity is found to be stronger in hover compared to the ascending flight. This quantity may be influenced by the dissipation of vorticity due to coarse mesh constructed below the rotor plane where an exponential point distribution was used.

The growth of the tip vortex core extracted for one rotor revolution is presented in Fig. 7a. It is found that, for the same mesh distribution, the core radius increases linearly with vortex age and grows faster in hovering flight. Similarly to the hovering cases, the tip vortex of an ascending rotor looks self-similar when the normalised swirl velocity of the core is plotted against the normalised radial distance (Fig. 7b).

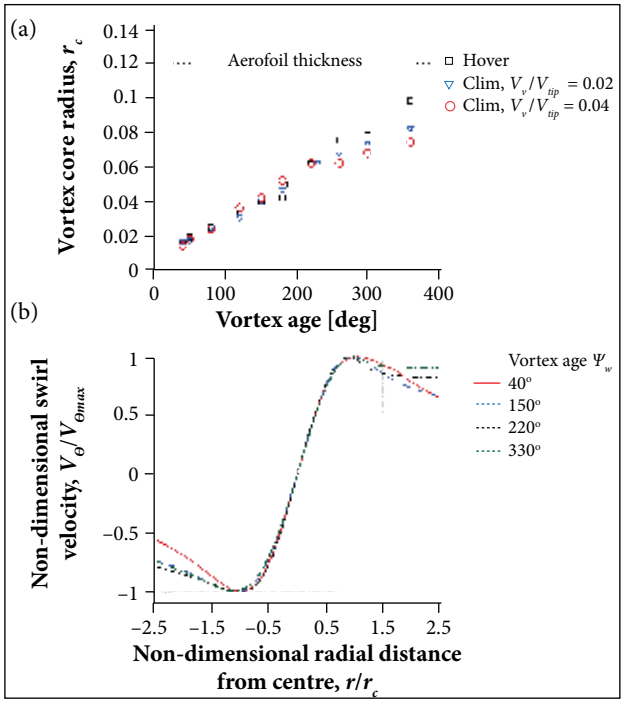

Figure 7. Predicted core growth and self-similarity of the UH-1H rotor tip vortices at different ascent rates. (a) Vortex core radius; (b) Vortex self-similarity.

DESCENDING WASHIZU ROTOR

Experiment for rotors in descending flight performed by Washizu et al. (1966) were referred in this study. In the experiment, the rotor was tested in a towing basin with the aim of eliminating the blockage effect that occurs in most wind tunnel experiments.

The experiments of the Washizu rotor in descending flight include hover, vortex-ring state ($V_v/Vt_{ip} = 0.054$, $V_v = 3.11$ m/s) and wind-mill brake state, WBS ($V_v/Vt_{ip} = 0.09$, $V_v = 5.184$ m/s), and these were computed using CFD. The test cases consider the blade tip Reynolds and Mach numbers fixed to a constant value of 1.306×10^6 and 0.1693, respectively. The rotor has 3 blades, and the blade collective pitch setting varied from 0°, 4.5° to 8°. The descending flight was simulated by increasing the descend speed while keeping the rotor tip speed constant. In CFD, the freestream far field boundary was specified for rotors in descending flight, and a Froude (source-sink) condition was used for the hovering flight case. The turbulence closure was achieved using the 2 equations of the k-ω model with transport of shear stress (SST) and baseline (BSL) variant. Figures 8a and 8b show the convergence history for rotor thrust and torque coefficients. It can be seen that rotor thrust and torque in WBS fluctuate even after 80,000 iteration steps. This behaviour is apparently caused by the highly separated flow developed on the upper blade surface. In descending flight, the rotor blades experience a flow coming from below the rotor plane.

The comparisons of the chordwise blade surface pressure at 3 blade stations (r/R = 0.3, 0.75, and 0.9) are presented in Fig. 9. The results suggest that the blade in VRS and WBS has large flow separation on the upper surface of the blade. This situation occurs up to r/R = 0.75. The chordwise plot of flow streamlines visualised at 3 blade stations are shown in

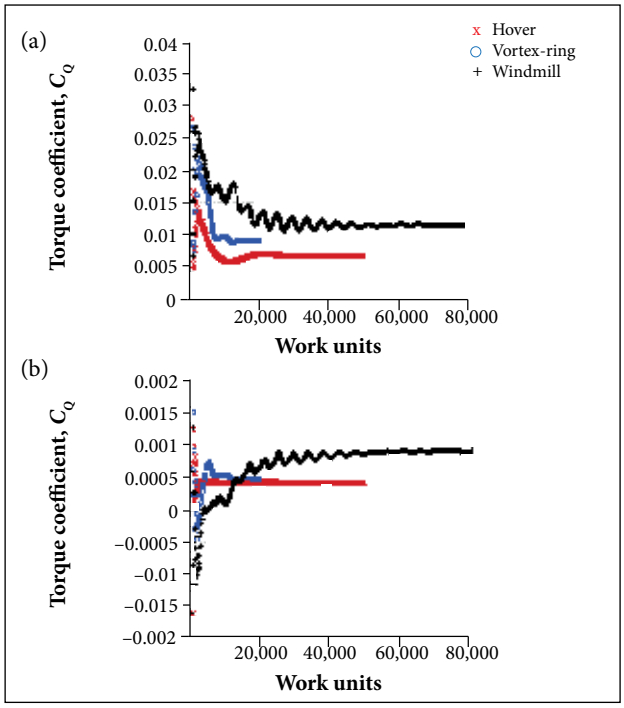

Figure 8. Convergence history plots for the Washizu rotor in descending flight ($\theta_{0.7}$ = 8°, M_{tip} = 0.1693). (a) Thrust history; (b) Torque history.

Figs. 10 and 11. As shown in Fig. 10, for the rotor in VRS, the blade at 20%*R* experiences leading edge separation and then growth to fully separated flow on the upper blade surface at 40%*R*. A much more severe flow separation can be verified for the blade in windmill brake as shown in Fig. 11, where almost 75%*R* of blade is separated.

For hovering rotor, the flow field enters the computational domain from all directions and is induced downstream below the rotor. In descending flight, however, the inflow velocity enters the domain from the boundary located below the rotor plane. In the VRS, where the transport of vorticity is approximately equal to the rate of descent, a large recirculation

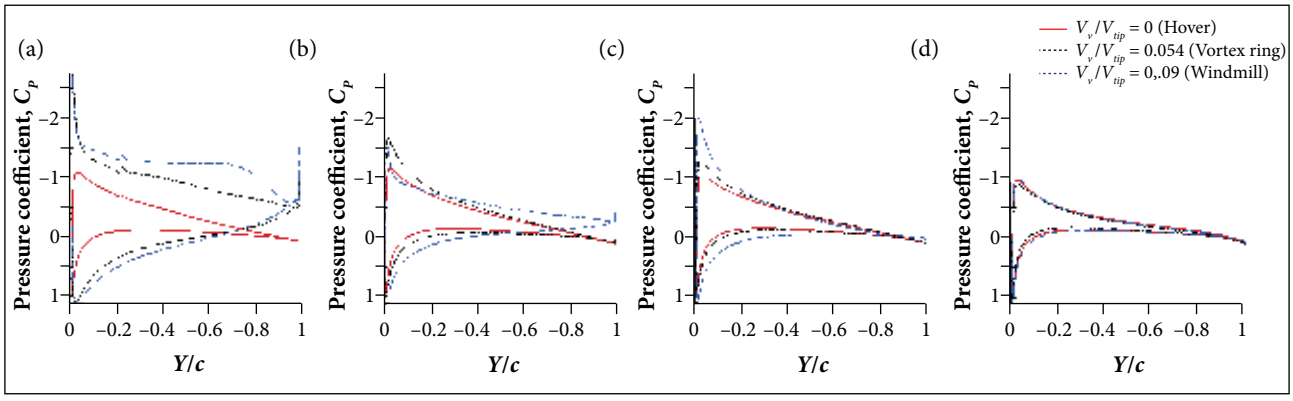

Figure 9. Comparison of CFD results of the Washizu rotor blade surface pressure coefficient at different descent rates ($\theta_{0.7}$ = 8°, M_{tip} = 0.1693). (a) *r*/*R* = 0.30; (b) *r*/*R* = 0.75; (c) *r*/*R* = 0.90; (d) *r*/*R* = 0.99.

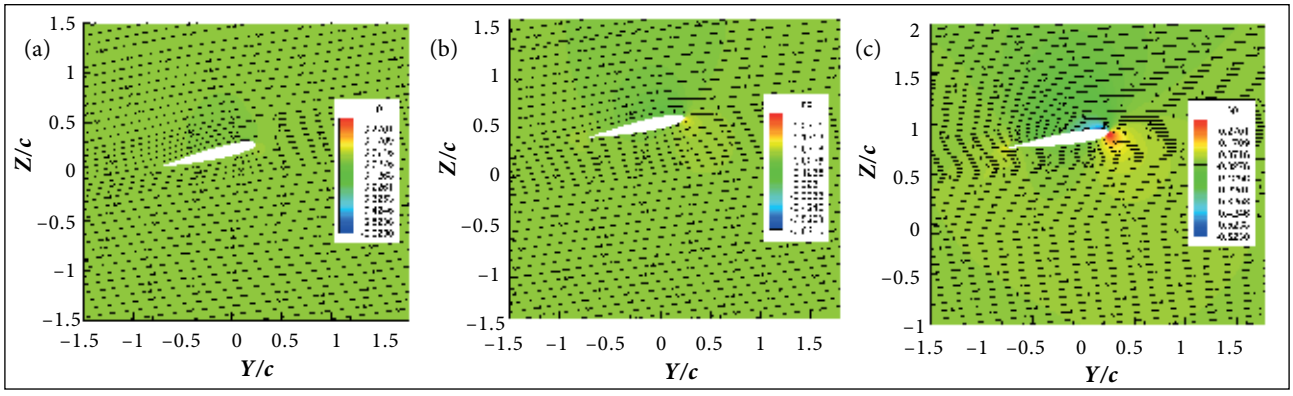

Figure 10. Streamlines and contour of pressure coefficient for rotor in VRS ($\theta_{0.75}$ = 8°, M_{tip} = 0.1693). (a) *r*/*R* = 0.20; (b) *r*/*R* = 0.40; (c) *r*/*R* = 0.70.

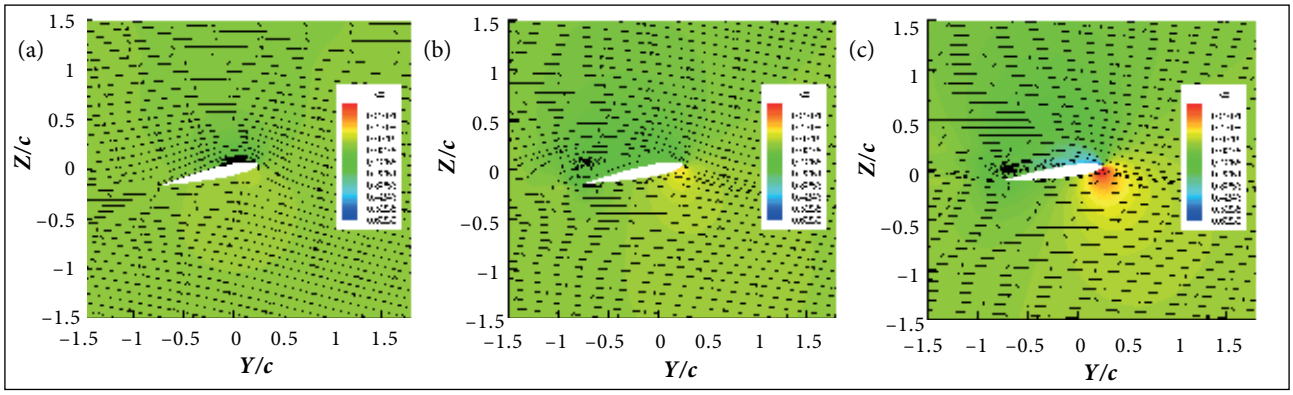

Figure 11. Streamlines and contour of pressure coefficient for rotor in WBS ($\theta_{0.75}$ = 8°, M_{tip} = 0.1693). (a) *r*/*R* = 0.20; (b) *r*/*R* = 0.40; (c) *r*/*R* = 0.70.

flow exists near the blade tip. Nevertheless, the mesh setting used was still unable to accurately capture the collection of tip vortices accumulated in this recirculation flow as found in most experiments. In the windmill brake state, where the rotor experiences a fast descent rate, the flow field continues to expand above the rotor plane. Iso-surfaces of Q-criterion coloured by pressure are depicted in Fig. 12. The Q-criterion is used here to visualise the highly concentrated vorticity regions by plotting the rotation-dominated strain in the flow. A large area of fully turbulence flow is seen to be developed around the rotor in WBS.

The comparisons of the rotor performance in terms of torque coefficient (C_Q) *versus* thrust coefficient (C_T) and FM *versus* C_T are given in Fig. 13. The effects of different turbulence models (k-ω BSL and SST) and trim conditions are also presented. The results suggest that, for low collective pitch settings, the CFD slightly overpredicts rotor torque for all test cases. Trimming the rotor improves the performance prediction compared to the untrimmed condition. Moreover, for a high collective pitch setting, a large offset of rotor torque was observed.

The FM of rotors in hover is plotted for different blade collective pitch settings in Fig. 13b. The CFD results show a well predicted FM for non-lifting rotor ($C_T = 0$), but this value is slightly below the experimental results for the 4.5° and 8° pitch settings. From these results, it can be concluded that the CFD method used can predict rotor performance in steep descent up to an acceptable accuracy.

Comparisons of the predicted rotor performance (trimmed condition) against momentum theory and experiments are shown in Fig. 14. As explained in the previous section, the rotor was trimmed to a specific thrust coefficient. The effect of trimming can be seen on the torque coefficient required to maintain the rotor descend speed for a particular rotor thrust and blade collective angles. There are discrepancies in torque prediction between CFD and the other 2 data. These could be due to potential errors in the experiments at high pitch angles and high rates of descent due to limited speed of the carriage, and the length of the track (Washizu *et al.* 1966).

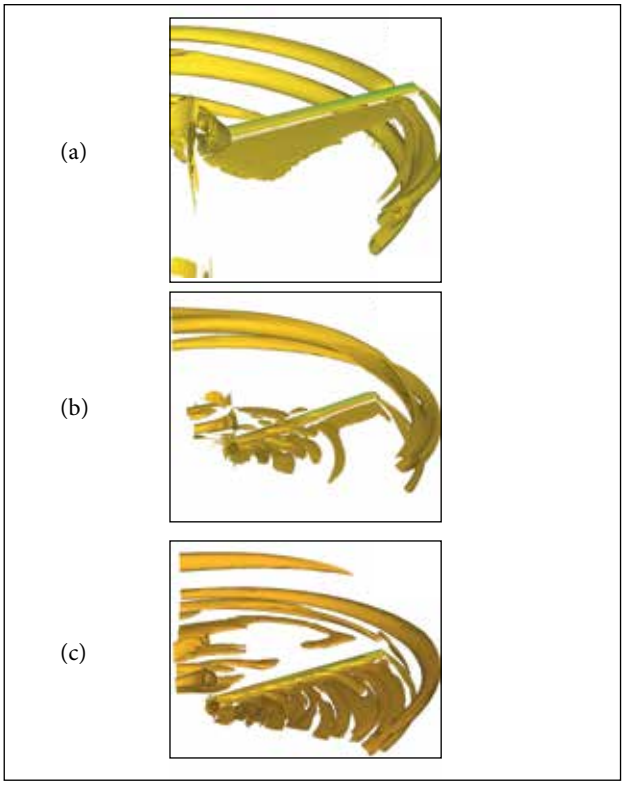

Figure 12. Vortical structures of rotors in descending flight visualised using iso-surface of Q-criterion coloured by pressure contour ($\theta_{0.75} = 8°$, $M_{tip} = 0.1693$). (a) $V_v/V_{tip} = 0$ (Hover); (b) $V_v/V_{tip} = 0.054$ (Vortex ring); (c) $V_v/V_{tip} = 0.09$ (Windmill brake).

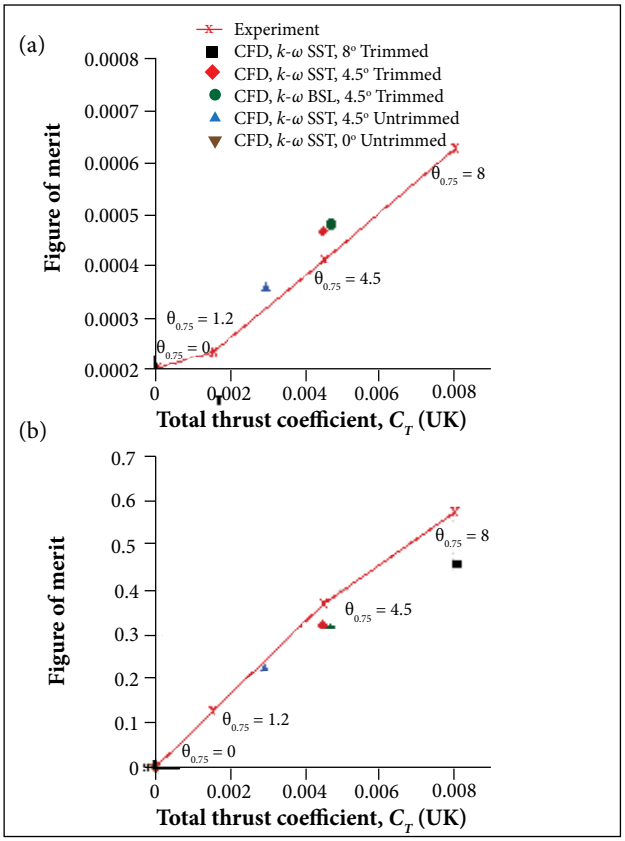

Figure 13. Performance of the Washizu rotor in hover. (a) C_T versus C_Q; (b) Figure of merit versus C_Q.

Furthermore, no detailed discussion on the hover and windmill test cases was given.

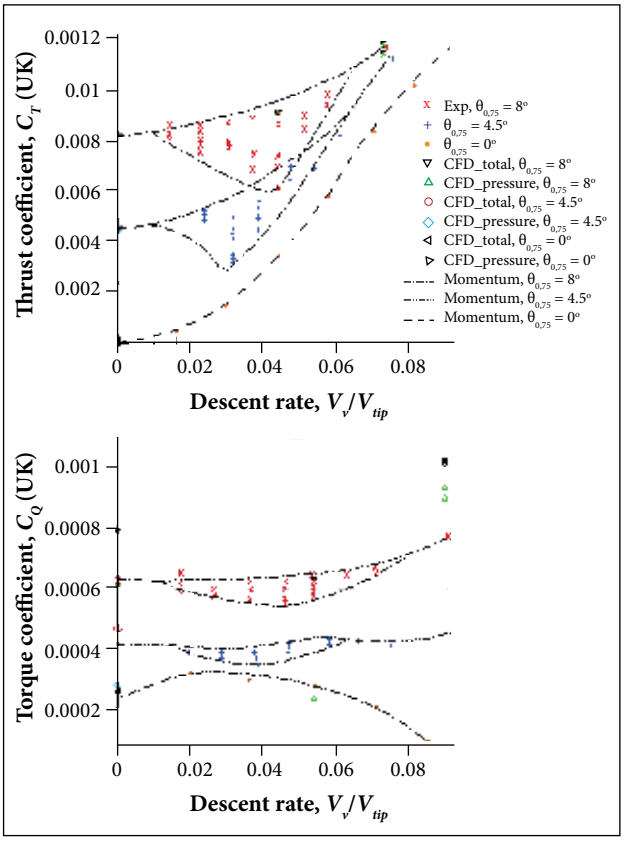

Figure 14. Comparison of the Washizu rotor performance plotted for different descent rates and collective pitch settings.

CONCLUSIONS

Accurate prediction of rotor blade aerodynamics in axial flight is a challenging task in computational fluid dynamics. This is due to the presence of large-scale vortical structures that interact with the blade near the tip and need to be accurately modelled. In this study, the performance of rotors in various axial flight conditions in vertical ascend, hover, and descent was computed using the Helicopter Multi-block (HMB) flow solver.

For rotors in hover and vertical ascend, the blade surface pressure, the integrated rotor performance, and the vortex wake trajectory were analysed using HMB and compared with the experimental data of the UH-1H rotor. It can be concluded that the HMB solver can predict well the blade aerodynamic performance in comparison to experimental and HELIX-I data. However, for low ascending rate, small discrepancies can be observed. This is expected due to the aperiodicity and recirculation of the flow field in the wind tunnel rather than CFD errors. Similar hover test cases were also employed for validation including the hovering Caradonna-Tung model rotor, with good success. For the same wake age considered, the distribution of the normalised vortex swirl velocity across the vortex core in climb was found to be weaker and smaller in radius than for the rotors in hover. Furthermore, the tip vortex showed more contraction in hover and fast descending than for ascending flight.

When the rotor descended into its own wake, a large flow separation developed on the upper surface of the blade extending up to 55%R. A more severe and chaotic flow field was observed for the rotor in windmill brake state where more than 75%R of the blade span experienced stall. The predictions of thrust and torque showed that the blade collective pitch had to be trimmed to the required thrust. The used of the baseline (BSL) and shear stress transport (SST) k–ω turbulence models showed little influence on the torque predictions.

Overall, the present work on rotors in axial flight has successfully validated the HMB solver using several rotor test data. The work presented, provides additional knowledge on rotor performance but there are still certain areas that are not well understood. Although CFD can be a good tool in predicting the basic flow physics on different axial flight regimes, future work and validation against new experiments are needed. This calls for experiments in various regimes of axial flight that should be the target of large international initiatives and should result in open databases of measurements.

ACKNOWLEDGEMENTS

The authors would like to acknowledge the Malaysian Ministry of Higher Education and Universiti Teknologi Malaysia for financial support for this research project.

AUTHOR'S CONTRIBUTION

Mohd NARN performed the numerical calculation and prepared the figures; Barakos G conceived the idea and co-wrote the main text. All authors discussed the results and commented on the manuscript.

REFERENCES

Ahlin GA, Brown RE (2005) Investigating the physics of rotor vortex ring state using the vorticity transport model. Proceedings of the 31st European Rotorcraft Forum; Florence, Italy.

Badcock K, Richards B, Woodgate M (2000) Elements of computational fluid dynamics on block structured grids using implicit solvers. Progr Aero Sci 36(5-6):351-392. doi: 10.1016/S0376-0421(00)00005-1

Bailly J (2010) A qualitative analysis of vortex ring state entry using full time marching unsteady wake model. Proceedings of the 34th European Rotorcraft Forum; Liverpool, UK.

Barakos G, Steijl R, Badcock K, Brocklehurst A (2005) Development of CFD capability for full helicopter engineering analysis. Proceedings of the 31st European Rotorcraft Forum; Florence, Italy.

Brand A, Drier M, Kisor R, Wood T (2011) The nature of vortex ring state. J Am Helicopter Soc 56:1-14. doi: 10.4050/JAHS.56.022001

Brinson P, Ellenrieder T (1998) The nature of vortex ring state. Proceedings of the 24th European Rotorcraft Forum; Marseille, France.

Brocklehurst A, Steijl R, Barakos G (2008) CFD for tail rotor design and evaluation. Proceedings of the 34th European Rotorcraft Forum; Liverpool, UK.

Caradonna FX (1999) Performance measurement and wake characteristics of a model rotor in axial flight. J Am Helicopter Soc 44(2):101-108. doi: 10.4050/JAHS.44.101

Caradonna FX, Tung C (1981) Experimental and analytical studies of a model helicopter rotor in hover. NASA-TM-81232.

Conlisk AT (2001) Modern helicopter rotor aerodynamics. Progr Aero Sci 37(5):419-476. doi: 10.1016/S0376-0421(01)00011-2

Drees JM, Hendal WP (1951) Airflow patterns in the neighbourhood of helicopter rotors: a description of some smoke tests carried out in a wind-tunnel at Amsterdam. Aircr Eng Aerosp Tech 23(4):107-111. doi: 10.1108/eb032021

Gagliardi A, Barakos GN (2008) Improving hover performance of low-twist rotors using trailing-edge flaps — a computational study. Proceedings of the 34th European Rotorcraft Forum; Liverpool, UK.

Green RB, Gillies EA, Brown RE (2005) The flow field around a rotor in axial descent. J Fluid Mech 534:237-261. doi: 10.1017/S0022112005004155

Johnson W (1980) Helicopter theory. Princeton: Princeton University Press.

Leishman JG (2006) Principles of helicopter aerodynamics. Cambridge: Cambridge University Press.

Line AJ, Brown RE (2004) Efficient high-resolution wake modelling using the vorticity transport equation. Proceedings of the 60th Forum of the American Helicopter Society; Baltimore, USA.

McAlister KW, Huang SS, Abrego AI (2001) A model rotor in axial flight. NASA/TM-2001-210925.

Menter FR (1994) Two-equation eddy-viscosity turbulence models for engineering applications. AIAA J 32(8):1598-1605. doi: 10.2514/3.12149

Nik Mohd NAR, Barakos GN (2010) Computational aerodynamics of hovering helicopter rotors. Proceedings of the 2010 RAeS Aerodynamics Conference; Bristol, United Kingdom.

Nik Mohd NAR, Barakos GN, Batrkov AS, Kusyumov AN, Nikolaev EI (2011) Computational aerodynamics of rotors in hover and vertical climb. Transactions of Academenergo 4:118-129.

Perry FJ, Chan WFY, Simon I, Brown RE, Ahlin GA, Khelifa BM, Newman SM (2007) Modelling the mean flow through a rotor in axial flight including vortex ring conditions. J Am Helicopter Soc 52(3):224-238. doi: 10.4050/JAHS.52.224

Srinivasan GR (1993) A free-wake Euler and Navier-Stokes CFD method and its application to helicopter rotors including dynamic stall. Mountain View: JAI Associates, Inc.; [accessed 2017 Jan 6]. http://oai.dtic.mil/oai/oai?verb=getRecord&metadataPrefix=html&identifier=ADA275416

Steijl R, Barakos G, Badcock K (2006) A framework for CFD analysis of helicopter rotors in hover and forward flight. Int J Numer Meth Fluid 51(8):819-847. doi: 10.1002/fld.1086

Wang SC (1990) Analytical approach to the induced flow of a helicopter rotor in vertical descent. J Am Helicopter Soc 35(1):92-97. doi: 10.4050/JAHS.35.92

Washizu K, Azuma A, Koo J, Oka T (1966) Experiments on a model helicopter rotor operating in the vortex ring state. J Aircraft 3(3):225-230. doi: 10.2514/3.43729